International Journal of Thermofluids 26 (2025) 101135

Contents lists available at ScienceDirect

International Journal of Thermofluids

journal homepage: www.sciencedirect.com/journal/international-journal-of-thermofluids

Fractional analysis for heat consumption of *CuO*-based hybrid nanofluid via integral transform

Firas Ghanim [a], Ali Hasan Ali [b,c,d,*], Ghassan Ezzulddin Arif [e], Ali Raza [f]

[a] Department of Mathematics, College of Sciences, University of Sharjah, Sharjah, United Arab Emirates
[b] Institute of Mathematics, University of Debrecen, Pf. 400, H-4002, Debrecen, Hungary
[c] Department of Business Management, Al-imam University College, Balad 34011, Iraq
[d] Technical Engineering College, Al-Ayen University, Dhi Qar 64001, Iraq
[e] Department of Mathematics, College of Education for Pure Sciences, Tikrit University, Tikrit, Iraq
[f] Department of Mathematics, Minhaj University Lahore, Pakistan

ARTICLE INFO

Keywords:
Fractal fractional
Hybrid nanofluid
Viscous flow
Channel flow
Porous medium

ABSTRACT

The article covers two other sources of solar energy: industrial devices and nanofluids, which are employed in thermal engineering. The article makes the case that thermal engineering and industrial solar energy technologies can generate solar energy from alternative sources, such as nanofluids. Fractal fractional derivatives are a new and modified type of fractional derivative that has been developed to solve issues with hybrid nanofluid suspension. Several numerical techniques, such as Stehfest's and Tzou's algorithms, and the integral transform method, also known as Laplace transformation, are used to examine the approximate solution of the governed PDEs. At various time values, the numerical impacts of heat and flow rate are discernible. We then deduced that the momentum and heat profiles decreased with increasing fractal limitations. Furthermore, the momentum and temperature gradients progressively rise close to the plate and fall away from it when all prerequisites are satisfied. Because of the physical relevance of the nanoparticles under consideration, the water-based (H_2O) solution also has a more obvious influence when comparing various nanofluids than the (*CMC*)-based hybrid nanofluid.

1. Introduction

In 1995, Choi was one of the first to introduce nanofluids containing nanoparticles [1]. Among the numerous advantages that nanofluids may offer is thermal conductivity. The fluid is referred to as a "nanofluid" when it is combined with nanoparticles of different sizes to form a colloidal solution. Water, oil, and ethylene glycol are frequently the basis fluids. Metals, oxides, carbides, and carbon nanotubes are frequently converted into nanoparticles using nanofluids. Base fluids are combined with two or more types of nanoparticles to create hybrid nanofluids. In heat transfer scenarios, hybrid nanofluids outperform the conventional fluids used for the purpose. Hybrid nanofluids can efficiently cool high temperatures and a range of thermal applications. One popular method for creating unique nanotechnology is to introduce two distinct kinds of nanoparticles into necessary fluids, which are called hybrid nanofluids. Usually, they are intended for Choi and Eastman's courses in mechanical design, fluid mechanics, and biomedical engineering [2]. Ali et al. [3] gave a presentation on the study of a physically shaky representation of hybrid viscous nanofluids as they are utilized for mass and heat transmission. Ahmad et al. [4] confirmed the arrangements for a simultaneous Casson nanofluid convection flow over an endless vertical plate. A convergent series solution was found by Hayat et al. [5], flowing by a stretched surface of Casson nanofluids. Electro-hydrodynamic nanofluid in a container with a sinusoidal top wall was studied by Ellahi et al. [6]. They discovered that when the intensity of the electric field grows, isotherms get denser, and heat transmission gets faster. The flow of nanofluids with different thermal conditions and perceptions was also investigated by Sheikholeslami et al. [7] using the Koo-Kleinstreuer-Li (KKL) correlation. In several scientific domains, fractional calculus has emerged as a useful tool in recent years. In every scientific study, non-integer derivatives are valued more highly than traditional calculus. Milici gave a brief introduction to fractional differential equations [8]. Diffusion, combustion, electrochemistry, fractional wavelets, geophysics, fractional filters, viscoelasticity, the generation of suspensions in medicine, microelectronics, and

---

* Corresponding author.
E-mail addresses: fgahmed@sharjah.ac.ae (F. Ghanim), ali.hasan@science.unideb.hu (A.H. Ali), ghasanarif@tu.edu.iq (G.E. Arif), maleraxa@gmail.com (A. Raza).

https://doi.org/10.1016/j.ijft.2025.101135

Nomenclature

Symbol Quantity Unit

$\boldsymbol{\theta}$: Inclined magnetic field (−)
$\boldsymbol{U_0}$: Characteristic velocity (ms^{-1})
$\boldsymbol{q}$: Laplace transform variable (−)
$\boldsymbol{\mu_{nf}}$: Dynamic viscosity (Kg/ms)
$\boldsymbol{\sigma}$: Electrical Conductivity (−)
$\boldsymbol{V_1}$: Fluid velocity (m/s)
$\boldsymbol{\alpha, \beta}$: Fractional parameters (−)
$\boldsymbol{Gr}$: Heat Grashof number (−)
$\boldsymbol{Gm}$: Mass Grashof number (−)
$\boldsymbol{M}$: Magnetic field (−)
$\boldsymbol{\rho_{nf}}$: Nano-fluid density (Kg/m^3)
$\boldsymbol{Nu}$: Nusselt number (−)
$\boldsymbol{Pr_{eff}}$: Prandtl number (−)
$\boldsymbol{B_o}$: Strength of Magnetic field (Kg/s^2)
$\boldsymbol{g}$: Gravity acceleration (m/s^2)
$\boldsymbol{Sh}$: Sherwood number (−)
$\boldsymbol{C_p}$: Specific heat at the constant pressure (J/kgK)
$\boldsymbol{Sc}$: Schmidt number (−)
$\boldsymbol{C_f}$: Skin friction (−)

the movement of magnetic particles in the blood are just a few of the scientific and technological applications of fractional order calculus. Nonlinear models and mathematical models utilizing integer order derivatives frequently execute unsatisfactorily.

Numerous disciplines, including fluid dynamics, electromagnetics, optics, signal processing, and viscoelasticity, use fractional calculus. Both the conceptual and physical forms have been demonstrated by it. It has been applied to demonstrate that the material and physical forms that may be present in a model may be best explained by fractional differential conditions. For the accurate modeling of those frameworks that call for the specialized modeling of damping, fractional derivative models are used, as discussed by Boutiara et al. [9], through antiperiodic edge situations in the framework of Caputo function-dependent kernel partial derivatives. Time-fractional natural circulation flow with Newtonian heating and mass diffusion was studied by Vieru et al. [10]. Temperature and velocity were found to be the growth functions of the fractional component. Aman et al. [11] have utilized the Caputo fractional technique to examine the heat transfer of water-based nanofluid flow. Fractional derivatives are crucial for researching fluid dynamics, economics, physics, and applied mathematics, claim Kulick et al. [12]. Ali et al. [13] employed Caputo-Fabrizio derivatives for the free convection flow in the MHD of the generalized Walter'-B fluid model. Because Azhar et al. [14] found that the momentum barrier layer was thicker with higher Prandtl numbers, they concluded that fractional nanofluids transfer heat more quickly than ordinary nanofluids.

Channel flow is the process by which the confining walls change the hydrodynamic structure of the flow from an unconstrained state at the channel entrance to a particular condition at the exit. The phrase "bio-convection" refers to the spectacular motion of macroscopic fluid induced by the thickness angle created by creatures swimming in a coordinated group. Plat proposed the notion of bio-convection in 1961. Convective heat transfer flow in a channel has captured the interest of researchers in fields such as thermal and nuclear power engineering. Recently, combining the effects of the radiative heat transfer, transverse magnetic field, and mixed convection flow has moved optically thin fluid along a conduit with heated bounding walls and saturated porous media [15–19]. The relevance of mixed convection and pulsatile Poiseuille flow (PPF), generally known as mixed convection PPF, could be understated. Mixed convection develops in channel flow when the channel walls are cooled or heated. A magnetic field that influences the Poiseuille flow and heat transfer of carbon nanotubes was examined by Eman et al. [20] in their evaluation of the impact of a vertical Casson fluid-filled conduit. Among the many uses for bioconvection are laboratory divisions, biotechnology, biosensors, testing, and the production of biological materials [21]. In areas such as thermal and nuclear power engineering, convective heat transfer flow in a channel has generated great curiosity. However, the relevance of mixed convection and pulsatile Poiseuille flow, generally known as mixed convection PPF, could be understated. Mixed convection develops in channel flow when the channel walls are cooled or heated.

Few studies on fractional derivatives nanofluids have been described, based on the literature mentioned above. As far as the authors are aware, the only recent work in this field on fractional Maxwell kinematic nanofluid over an inclined plate employing Caputo fractional definition was published by Cao et al. [22]. Ali et al. [23] conducted another investigation. They used the Prabhakar fractional definition to solve the problem, which involved Ag and CuO with water as the base fluid. Recent studies on fractional nanofluids may be found in [24–27] and their citations. This most recent field encouraged us to use a fractional derivative approach to study an issue involving nanofluids. This study aim is: what effects do fractal fractional limitations have on hybrid nanofluids' momentum and thermal behavior?. In the areas of heat transmission and flow properties, what are the relative benefits of hybrid nanofluids according to water and CMC?. How are the momentum and temperature fields in hybrid nanofluids affected by the direction and strength of the magnetic field?. Using the most recent description of the fractional derivative the fractal fractional derivative and its utilization is our goal here. Additionally, to use various numerical methods to assess the increase of the heat transfer rate and analyze the problem's physical understanding using graphs.

2. Mathematical problem description

Consider an unsteady, free convective, and incompressible hybrid nanofluid flow in a vertical channel of *CMC* and H_2O-based nanofluid with silver (*Ag*) and copper-oxide (*CuO*) nanoparticles. The flow with an inclination of angle direction (θ) is implemented using a continuous magnetic field of intensity B_0. Even though the whole system is at rest during time $t = 0$. After some time, the static plates oscillate, and the temperature field varies with time, as can be seen in Fig. 1; this causes static fluid to start to flow. The energy equation does not take into account viscous dissipation. While ψ_0 and ψ_d stand in for the left and right plates' concentrations, ϑ_0 and ϑ_d in the vertical channel indicate the plates' temperature, respectively. The following assumptions for the coming model are as follows:

- Parallel plates have an infinite length at the width d.
- The plates (poured) are oriented along the $x - axis$ and perpendicular to $y - axis$.
- Initially, both concentration and temperature are fixed to constant as ψ_o and ϑ_o, respectively, at time $t = 0$.
- Various nanoparticle-merged hybrid nanofluids accelerate along the x-axis.
- A magnetic field with a constant strength of B_o exists near the flowing fluid.

The Roseland [28] and Boussinseq approximations [29] may be used to write the governed partial differential equations as follows [11]:

$$\rho_{nf}\frac{\partial V_1(\xi,t)}{\partial t}=\mu_{nf}\frac{\partial^2 V_1(\xi,t)}{\partial \xi^2}+g(\rho\beta_T)_{nf}(\vartheta_1(\xi,t)-\vartheta_o)-\left(\sigma_{nf}B_o^2 sin(\theta)+\frac{\mu_{nf}\varphi}{k_1}\right)V_1(\xi,t)$$
$$+g(\rho\beta_c)_{nf}(\psi_1(\xi,t)-\psi_o), \tag{1}$$

$$(\rho C_p)_{nf}\frac{\partial\vartheta_1(\xi,t)}{\partial t}=\frac{\partial^2\vartheta_1(\xi,t)}{\partial\xi^2}+4\alpha_o^2(\vartheta-\vartheta_o), \tag{2}$$

$$\frac{\partial\psi_1(\xi,t)}{\partial t}=D_{nf}\frac{\partial^2\psi_1(\xi,t)}{\partial\xi^2}. \tag{3}$$

Here, $\frac{\partial q_r}{\partial \xi}=4\alpha_o^2(\vartheta_1-\vartheta_o)$ represents the radiant heat flow with the given boundary conditions,

$$V_1(\xi,0)=0,\ \vartheta_1(\xi,0)=\vartheta_o,\ \psi_1(\xi,0)=\psi_o, \tag{4}$$

$$V_1(0,t)=V_o,\ \vartheta_1(0,t)=\vartheta_o,\ \psi_1(0,t)=\psi_0, \tag{5}$$

$$V_1(1,t)=V_o,\ \vartheta_1(1,t)=\vartheta_d,\ \psi_1(1,t)=\psi_d, \tag{6}$$

and the non-dimensional constraints are as follows [11]:

$$\xi^*=\frac{\xi}{d},\ V_1^*=\frac{V_1}{U_o},\ t^*=\frac{U_o^2}{\upsilon_f}t,$$

$$\vartheta_1^*=\frac{\vartheta_1-\vartheta_o}{\vartheta_d-\vartheta_o}=\frac{\vartheta_1-\vartheta_o}{\Delta\vartheta},\ \psi_1^*=\frac{\psi_1-\psi_o}{\psi_d-\psi_o}=\frac{\psi_1-\psi_o}{\Delta\psi}.$$

Substituting (1) through (6) for the governing equations and conditions and by eliminating the steric notation, we determine the following non-dimensional governed equations:

$$\Omega_1 Re\frac{\partial V_1(\xi,t)}{\partial t}=\Omega_2\frac{\partial^2 V_1(\xi,t)}{\partial\xi^2}-\left(M\ sin(\theta)+\frac{\Omega_2}{K}\right)V_1(\xi,t)+\Omega_3 Gr\vartheta_1(\xi,t)$$
$$+\Omega_4 Gm\ \psi_1(\xi,t), \tag{7}$$

$$Pe\ \frac{\partial\vartheta_1(\xi,t)}{\partial t}=\frac{\partial^2\vartheta_1(\xi,t)}{\partial\xi^2}+N^2\vartheta_1(\xi,t), \tag{8}$$

$$b_3\frac{\partial\psi_1(\xi,t)}{\partial t}=\frac{\partial^2\psi_1(\xi,t)}{\partial\xi^2}, \tag{9}$$

and the succeeding dimensionless conditions

$$V_1(\xi,0)=0,\ \vartheta_1(\xi,0)=0,\ \psi_1(\xi,0)=0, \tag{10}$$

$$V_1(0,t)=0,\ \vartheta_1(0,t)=0,\ \psi_1(0,t)=0, \tag{11}$$

$$V_1(1,t)=0,\ \vartheta_1(1,t)=1,\ \psi_1(1,t)=1, \tag{12}$$

In order to properly depict the system's physical characteristics, the boundary conditions (10–12) were used. Condition (10) shows that the velocity V_1, temperature ϑ_1, and concentration ψ_1 are all zero across the entire domain at the starting time ($t=0$), indicating that there is no motion. At the boundary ($\xi=0$), condition (11) reduces all profiles to zero, signifying a thermally isolated and non-slip surface. In order to simulate a thermal and mass flux at the outermost layer, condition (12) states that the ϑ_1 and ψ_1 have been set to their maximum values although V_1 stays at zero at the boundary ($\xi=1$). These prerequisites

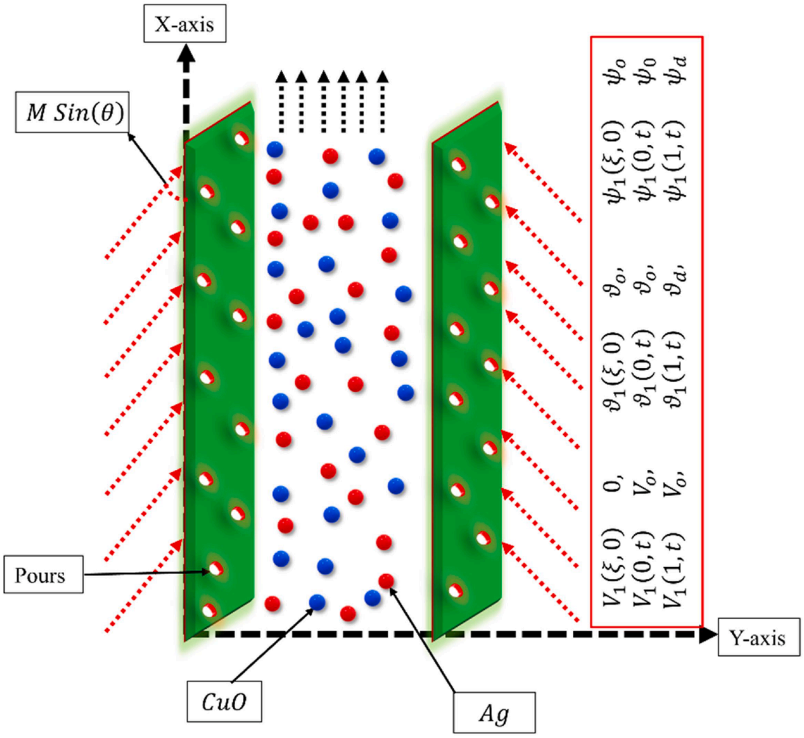

Fig. 1. Flow geometry.

guarantee that the model complies with physical limitations and accurately depicts the behavior of hybrid nanofluids both close to and far from the limits. Wherer

$$Pr = \frac{(\mu C_p)_f}{\kappa_f},\ Sc = \frac{\upsilon_f}{D},\ Gr = \frac{g(\beta_T)_f d^2(\vartheta_d - \vartheta_o)}{\nu U_o},\ K = \frac{k_1}{d},$$

$$Re = \frac{U_o d}{\nu},\ M = \frac{\sigma_f B_o^2 d^2}{\mu},\ Gm = \frac{g(\beta_c)_f d^2 \Delta\psi}{\nu U_o},\ N^2 = \frac{4\alpha_o^2 d^2}{k_f},$$

represents the Prandtl number, Schmidt number, heat Grashof number, porosity, Reynolds number, magnetic, Mass Grashof number, and radiation, respectively. Tables 1 and 2 list the thermophysical properties of NFs quantities, and the considered nanofluids with their thermal characteristics, respectively.

Silver (Ag) and copper oxide (CuO) nanoparticles were chosen because of their remarkable thermal characteristics, that render them ideal for hybrid nanofluid usage. CuO's strong heat conductivity, chemical reactivity, and affordability are well known. CuO is a perfect fit for a variety of thermal control technologies because of these characteristics, which allow for effective heat transmission. However, among metals, silver (Ag) nanoparticles have one of the strongest thermal conductivity rates, which greatly improves the nanofluid's capacity for heat transmission. Ag nanoparticles also have outstanding antibacterial and solubility stability, which gives the nanofluid additional multipurpose benefits.

Because water (H_2O) and carboxymethyl cellulose (CMC) support each other and improve the functionality of hybrid nanofluids, the pairing in the model under discussion is physically realistic. Because of its availability, low viscosity, and excellent heat conductivity, water is frequently employed as a base fluid in thermal structures. By making the fluid more stable and viscous, promoting even dispersion of the nanoparticles, and decreasing agglomeration, CMC, a water-soluble polymer, enhances the fluid's rheological characteristics.

3. Basic definitions

The power law for the continuous function y(x) may be described in terms of RL-form as follows:

$$^{FFP}D_x^{\alpha,\ \beta}y(x) = \frac{1}{\Gamma(1-\alpha)}\frac{d}{dx^\beta}\int_0^x y(t)(x-t)^{-\alpha}dt,\ 0<\alpha,\ \beta\le 1 \qquad (13)$$

$$\frac{dy(t)}{dx^\beta} = \lim_{x\to t}\frac{y(x)-y(t)}{x^\beta - t^\beta}.$$

Laplace Transformation: Consider $y(x)$ for instance where$(x>0)$. The Laplace integral offers a well-defined continuous function called the LT of $y(x)$ as $Y(s)$ or $\mathscr{L}\{y(x)\}$

$$\mathscr{L}\{y(x)\} = Y(x) = \int_0^\infty exp(-sx)f(x)dx. \qquad (14)$$

Fractal Laplace Transformation: The fractal-Laplace of the continuous function $g(x)$ can be defined as [32]:

$$^{F}\mathscr{L}_p^\alpha\{g(x)\} = G(x) = \int_0^\infty exp(-sx)x^{\alpha-1}g(x)dx. \qquad (15)$$

3.1. Fractal fractional model

For the guided problem, the fractional model can be employed as:

$$\frac{\Omega_1 Re}{\beta t^{\beta-1}}\,{}^{C}D_t^\alpha V_1(\xi,t) = \Omega_2\frac{\partial^2 V_1(\xi,t)}{\partial\xi^2} - \left(M\sin(\theta) + \frac{\Omega_2}{K}\right)V_1(\xi,t) + \Omega_3 Gr\vartheta_1(\xi,t) + \Omega_4 Gm\,\psi_1(\xi,t) - \frac{V_1(\xi,0)}{\Gamma(1-\alpha)}t^{-\alpha}, \qquad (16)$$

$$\frac{Pe}{\beta t^{\beta-1}}\,{}^{C}D_t^\alpha\ \vartheta_1(\xi,t) = \frac{\partial^2\vartheta_1(\xi,t)}{\partial\xi^2} + N^2\vartheta_1(\xi,t) - \frac{\vartheta_1(\xi,0)}{\Gamma(1-\alpha)}t^{-\alpha}, \qquad (17)$$

$$\frac{b_3}{\beta t^{\beta-1}}\psi_1(\xi,t) = \frac{\partial^2\psi_1(\xi,t)}{\partial\xi^2} - \frac{\psi_1(\xi,0)}{\Gamma(1-\alpha)}t^{-\alpha}. \qquad (18)$$

The flow chart of the whole study and methodology is shown in Fig 2.

4. Fractional solution

4.1. Expressions for temperature

Use the LT on Eq. (17) and associated conditions for the heat equation simulations as follows:

$$q^\alpha\overline{\vartheta}_1(\xi,q) - \overline{\vartheta}_1(\xi,0) = \beta\Gamma(\beta)\,q^{-\beta}\left\{\frac{1}{Pe}\frac{\partial^2\overline{\vartheta}_1(\xi,q)}{\partial\xi^2}\right\} + \beta\Gamma(\beta)\,q^{-\beta}\left\{\frac{1}{Pe}N^2\overline{\vartheta}_1(\xi,q)\right\} - \frac{\overline{\vartheta}_1(\xi,0)}{\Gamma(1-\alpha)}q^{-\alpha}\Gamma(1-\alpha), \qquad (19)$$

with

$$\overline{\vartheta}_1(1,q) = \frac{1}{q},\ \overline{\vartheta}_1(0,q) = 0. \qquad (20)$$

Using the pre-existing conditions to determine the heat flux solution, the following will be done:

$$\overline{\vartheta}_1(\xi,q) = \frac{1}{q}\ \frac{e^{\xi\sqrt{\frac{Pe}{\beta\Gamma(\beta)}q^{\alpha+\beta}-N^2}} - e^{-\xi\sqrt{\frac{Pe}{\beta\Gamma(\beta)}q^{\alpha+\beta}-N^2}}}{e^{\sqrt{\frac{Pe}{\beta\Gamma(\beta)}q^{\alpha+\beta}-N^2}} - e^{-\sqrt{\frac{Pe}{\beta\Gamma(\beta)}q^{\alpha+\beta}-N^2}}} = \frac{1}{q}\ \frac{Sinh\left[\xi\sqrt{\frac{Pe}{\beta\Gamma(\beta)}q^{\alpha+\beta} - N^2}\right]}{Sinh\left[\sqrt{\frac{Pe}{\beta\Gamma(\beta)}q^{\alpha+\beta} - N^2}\right]}. \qquad (21)$$

For the inverse of (21), we will use numerical approaches like Tzou's and Stehfest's systems, as shown in Tables 3 and 4.

4.2. Expressions for concentrations

Using the LT to the governed equations is similar to applying the energy Eqs. (9) and (19)

$$q^{\alpha}\overline{\psi}_1(\xi,q)-\overline{\psi}_1(\xi,0)=\beta\,\Gamma(\beta)\;q^{-\beta}\left\{\frac{1}{b_3}\frac{\partial^2\overline{\psi}_1(\xi,q)}{\partial\xi^2}\right\}-\frac{\overline{\psi}_1(\xi,0)}{\Gamma(1-\alpha)}q^{-\alpha}\Gamma(1-\alpha), \tag{22}$$

with conditions

$$\overline{\psi}_1(1,q)=\frac{1}{q},\;\overline{\psi}_1(0,q)=0.$$

Applying the above conditions, the concentration field's solution takes the following form

$$\overline{\psi}_1(\xi,q)=\frac{1}{q}\;\frac{e^{\xi\sqrt{\frac{b_3}{\beta\Gamma(\beta)}q^{\alpha+\beta}}}-e^{-\xi\sqrt{\frac{b_3}{\beta\Gamma(\beta)}q^{\alpha+\beta}}}}{e^{\sqrt{\frac{b_3}{\beta\Gamma(\beta)}q^{\alpha+\beta}}}-e^{-\sqrt{\frac{b_3}{\beta\Gamma(\beta)}q^{\alpha+\beta}}}}=\frac{1}{q}\;\frac{Sinh\left[\xi\sqrt{\frac{b_3}{\beta\Gamma(\beta)}q^{\alpha+\beta}}\right]}{Sinh\left[\sqrt{\frac{b_3}{\beta\Gamma(\beta)}q^{\alpha+\beta}}\right]}\;. \tag{23}$$

Different numerical techniques, such as Tzou's and Stehfest's [31], will be used in Tables (3 and 4) to calculate the inverse of Laplace's Eq. (23).

4.3. Expressions for velocity

The method applied in this section has also been utilized to solve the concentration and the energy profiles. The governed Eq. (7), along with the LT approach, allow us to derive:

The inverse Laplace transform is a fundamental tool in many fields, and numerous numerical techniques have been developed to approximate it. In this work, we employed Stehfest's method to numerically compute the momentum and thermal fields [30]. The mathematical formulation of the Gaver-Stehfest approach is expressed as:

$$h(y,t)=\frac{ln(2)}{t}\;\sum_{i=1}^{N}w_i\;\overline{h}\left(y,i\frac{ln(2)}{t}\right),$$

where the weights w_i are calculated as:

$$w_i=(-1)^{i+\frac{N}{2}}\sum_{l=\left[\frac{m+1}{2}\right]}^{min\left(m,\frac{N}{2}\right)}\frac{(2l)!l^{\frac{N}{2}}}{l!\;(2l-m)!\left(\frac{N}{2}-l\right)!(l-1)!(m-l)!}.$$

Here, $\overline{h}(y,s)$ represents the Laplace transform of the function $h(y,t)$, and the parameters N and m are chosen to optimize numerical accuracy. To validate the results obtained using Stehfest's method, we also applied Tzou's approach, an alternative numerical technique for approximating the inverse Laplace transform. Tzou's method is mathematically described as:

$$h(y,t)=\frac{e^{4.7}}{t}\left[\frac{1}{2}\overline{h}\left(s,\frac{4.7}{t}\right)+Re\left\{\sum_{k=1}^{N}(-1)^k\;\overline{h}\left(s,\frac{4.7+k\pi i}{t}\right)\right\}\right].$$

$$\begin{aligned}&\Omega_1 Re q^{\alpha}\overline{V}_1(\xi,q)-\overline{V}_1(\xi,0)\\&=\beta\,\Gamma(\beta)\;q^{-\beta}\left\{\Omega_2\frac{\partial^2\overline{V}_1(\xi,t)}{\partial\xi^2}-\left(M\;sin(\theta)+\;\frac{\Omega_2}{K}\right)\overline{V}_1(\xi,t)++\Omega_3 Gr\overline{\vartheta}_1(\xi,t)+\Omega_4 Gm\;\overline{\psi}_1(\xi,t)\right\}\\&-\beta\;\Gamma(\beta)\;q^{-\beta}\frac{\overline{V}_1(\xi,0)}{\Gamma(1-\alpha)}q^{-\alpha}\Gamma(1-\alpha),\end{aligned} \tag{24}$$

with

$$\overline{V}_1(0,q)=0,\;\overline{V}_1(1,q)=0.$$

Using the above conditions, we yield

$$\begin{aligned}\overline{V}_1(\xi,q)=&\left(\begin{aligned}&\frac{\Omega_3\;Gr}{\Omega_{22}\;q}\frac{1}{\left(\Lambda_o\;Pe\Lambda_2\;q^{\alpha+\beta}-N^2\right)-\frac{1}{\Omega_2}\left(M\;sin(\theta)+\frac{\Omega_2}{K}+\Omega_1 Re\;q^{\alpha+\beta}\right)}\\&+\frac{\Omega_4\;Gm}{\Omega_2 q}\frac{1}{\left(b_3\;\Lambda_o\;q^{\alpha+\beta}\right)-\frac{1}{\Omega_2}\left(M\;sin(\theta)+\frac{\Omega_2}{K}+\Omega_1 Re\;q^{\alpha+\beta}\right)}\end{aligned}\right)\\&\frac{Sinh\left[\xi\sqrt{\frac{1}{\Omega_2}\left(M\;sin(\theta)+\frac{\Omega_2}{K}+\Omega_1 Re\;q^{\alpha+\beta}\right)}\right]}{Sinh\left[\sqrt{\frac{1}{\Omega_2}\left(M\;sin(\theta)+\frac{\Omega_2}{K}+\Omega_1 Re\;q^{\alpha+\beta}\right)}\right]}\\&-\frac{a_3\;Gr}{a_2 q}\frac{1}{\left(\Lambda_o\;Pe\;q^{\alpha+\beta}-N^2\right)-\frac{1}{\Omega_2}\left(M\;sin(\theta)+\frac{\Omega_2}{K}+\Omega_1 Re\;q^{\alpha+\beta}\right)}\frac{Sinh\left[\xi\sqrt{\Lambda_o\;Pe\;q^{\alpha+\beta}-N^2}\right]}{Sinh\left[\sqrt{\Lambda_o\;Pe\;q^{\alpha+\beta}-N^2}\right]}\\&-\frac{a_4\;Gm}{a_2 q}\frac{1}{\left(b_3\;\Lambda_o\;q^{\alpha+\beta}\right)-\frac{1}{\Omega_2}\left(M\;sin(\theta)+\frac{\Omega_2}{K}+\Omega_1 Re\;q^{\alpha+\beta}\right)}\frac{Sinh\left[\xi\sqrt{b_3\;\Lambda_o\;q^{\alpha+\beta}}\right]}{Sinh\left[\sqrt{b_3\;\Lambda_o\;q^{\alpha+\beta}}\right]}.\end{aligned} \tag{25}$$

This formulation involves a combination of real and complex evaluations of the Laplace transform, leveraging exponential scaling for stability. The term $Re(.)$ denotes the real part of the summation. Both methods allow us to approximate the time-domain solution $h(y,t)$ with

Table 1

The thermophysical properties of NFs quantities are represented by [30].

Thermal features	Hybrid nanofluid
Density	$\rho_f = \dfrac{\rho_{hnf}}{\left((1-\varphi_2)\left((1-\varphi_1)+\varphi_1\dfrac{\rho_{s1}}{\rho_f}\right)+\varphi_2\rho_{s2}\right)}$
Dynamic Viscosity	$\mu_f = \mu_{hnf}(1-\varphi_1)^{2.5}(1-\varphi_2)^{2.5}$
Electrical conductivity	$\sigma_{bf} = \dfrac{\sigma_{hnf}}{\left(1+\dfrac{3\varphi\left(\varphi_1\sigma_1+\varphi_2\sigma_2-\sigma_{bf}(\varphi_1+\varphi_2)\right)}{\left(\varphi_1\sigma_1+\varphi_2\sigma_2+2\varphi\sigma_{bf}-\varphi\sigma_{bf}\left(\varphi_1\sigma_1+\varphi_2\sigma_2-\sigma_{bf}(\varphi_1+\varphi_2)\right)\right)}\right)}$
Thermal conductivity	$k_{bf} = \dfrac{k_{hnf}}{\left(\dfrac{k_{s2}+(n-1)k_{bf}-(n-1)\left(k_{bf}-k_{s2}\right)\varphi_2}{k_{s2}+(n-1)k_{bf}+\left(k_{bf}-k_{s2}\right)\varphi_2}\right)}$ and $k_f = \dfrac{k_{bf}}{\left(\dfrac{k_{s1}+(n-1)k_f-(n-1)\left(k_f-k_{s1}\right)\varphi_1}{k_{s1}+(n-1)k_f+\left(k_f-k_{s1}\right)\varphi_1}\right)}$
Heat capacitance	$\left(\rho C_p\right)_s = \dfrac{\left(\rho C_p\right)_{hnf}}{(1-\varphi_2)\left((1-\varphi_1)+\varphi_1\dfrac{\left(\rho C_p\right)_{s1}}{\left(\rho C_p\right)_f}\right)+\varphi_2\left(\rho C_p\right)_{s2}}$
Thermal Expansion Coefficient	$(\rho\beta)_f = \dfrac{(\rho\beta)_{hnf}}{(1-\varphi_2)\left((1-\varphi_1)+\varphi_1\dfrac{(\rho\beta)_{s1}}{(\rho\beta)_{f1}}\right)+\varphi_2(\rho\beta)_{s2}}$

Table 2

Considered nanofluids with their thermal characteristics [31].

Material	CMC	H_2O	CuO	Ag
$\boldsymbol{\rho(kg/m^3)}$	997	997.1	6320	10,500
$\boldsymbol{C_p(J/kgK)}$	4179	4179	531.8	235
$\boldsymbol{k(W/mK)}$	0.613	0.613	76.5	429
$\boldsymbol{\beta_T(K^{-1})}$	70×10^{-5}	21×10^{-5}	1.80×10^{-5}	1.89×10^{-4}

high accuracy, providing reliable estimates of the heat and momentum fields in the studied system.

4.4. Skin friction, Nusselt number, and Sherwood number

$$C_f = -\frac{\partial \overline{V}_1(\xi,q)}{\partial \xi}\bigg|_{\xi=0} = -\mathscr{L}^{-1}\left\{\frac{\partial V_1(0,t)}{\partial \xi}\right\},$$

$$Nu = -\frac{\partial \overline{\vartheta}_1(\xi,q)}{\partial \xi}\bigg|_{\xi=0} = -\mathscr{L}^{-1}\left\{\frac{\partial \vartheta_1(0,t)}{\partial \xi}\right\},$$

$$Sh = -\frac{\partial \overline{\psi}_1(\xi,q)}{\partial \xi}\bigg|_{\xi=0} = -\mathscr{L}^{-1}\left\{\frac{\partial \psi_1(0,t)}{\partial \xi}\right\},$$

5. Results discussion

The impact of MHD mixed convection flow of sodium carboxymethyl cellulose (CMC) and water (H_2O) as base fluid with silver (Ag) and copper-oxide (CuO) as base nanoparticles are briefly investigated in a suitable channel of a porous material. Numerous numerical solutions exist for the following variables: temperature, concentration, velocity field, and Nusselt number. This section examines the novel fractal fractional simulations for heat transport of mixed (CuO) and (Ag) nanofluid flowing through a vertically poured conduit. When a physical process changes, nanofluid behavior is demonstrated by altering some limitations while maintaining others. Figs. 3–11 illustrate the fractional nanofluid's flow, concentration, and temperature as functions of various parameters.

During changes in the physical process, the impact of the hybrid nanofluid is exhibited by holding some of the embedded parameters constant while modifying others. The effect of a fractional variable and Peclet number on fluid temperature are seen in Fig. 3(a, b). As the fractional parameter increases, the nanofluid's temperature decreases. By accounting for non-integer expansion self-replication, and memory impacts that are not taken into consideration by classical models, the fractal-fractional approach makes it possible to characterize variations in temperatures in intricate structures with more accuracy. At all scales of measure, the fractal-fractional technique is especially helpful in answering empirical issues pertaining to heat transport characteristics in irregular structures. In the study of fluid mechanics and thermal transport, the Peclet number (Pe) is without a dimension number. It highlights the relevance of advection in relation to dispersion in a system. The (Pe) is frequently used in the framework of heat exchange and the temperature field to comprehend how the movement of a fluid influences the temperature distribution. As a result, when (Pe) increases, the thermal field diminishes. Furthermore, the water-based ($CuO + Ag + H_2O$) hybrid nanofluid has a significantly more thermal profile than the CMC-based ($CuO + Ag + CMC$) hybrid nanofluid because of the physical significance of the investigated nanoparticles. The nanofluid concentration decreases when the fractional parameter (α) and volume fraction (φ) are increased, as seen in Fig. 4(a, b).

Non-integer development, self-simulation, and effects of memory that are not taken into consideration in traditional approaches are captured by fractional parameter (α). The concentration profile is influenced by the nanoparticle volume fraction (φ). In general, concentration profiles decline with increasing volume fractions. In a variety of applications, this modification enables more accurate concentration monitoring. More significant solid particle volume fractions enhance their amount in the solution by altering the local concentration dispersion. As a result of the enhancement of both constraints (α, φ), the concentration field will decline. Like the thermal field, the water-based ($CuO + Ag + H_2O$) hybrid nanofluid has a significantly more concentration field than the CMC-based ($CuO + Ag + CMC$) hybrid nanofluid.

As the fractional parameter increases, the fluid's velocity decreases, as shown by the graph in Fig. 5a. It results from the momentum boundary layer's thinner thickness compared to the thermal boundary layer in this situation. Fig. 5b shows the radiation parameter's velocity profile. This illustrates how increasing the value of the radiation parameter causes the fluid's velocity to increase. The proportional contribution of conductivity heat exchange to the distribution of thermal radiation is physically indicated by the radiation parameter N. As the radiation parameter increases, so does the boundary layer. As radiation parameters rise, the boundary layer's temperature rises as well. Again, like the thermal and concentration field, the impact of ($CuO + Ag + CMC$)-based hybrid nanofluid is somewhat lower as compared to ($CuO + Ag + H_2O$)-based hybrid nanofluid. The effect of the porosity

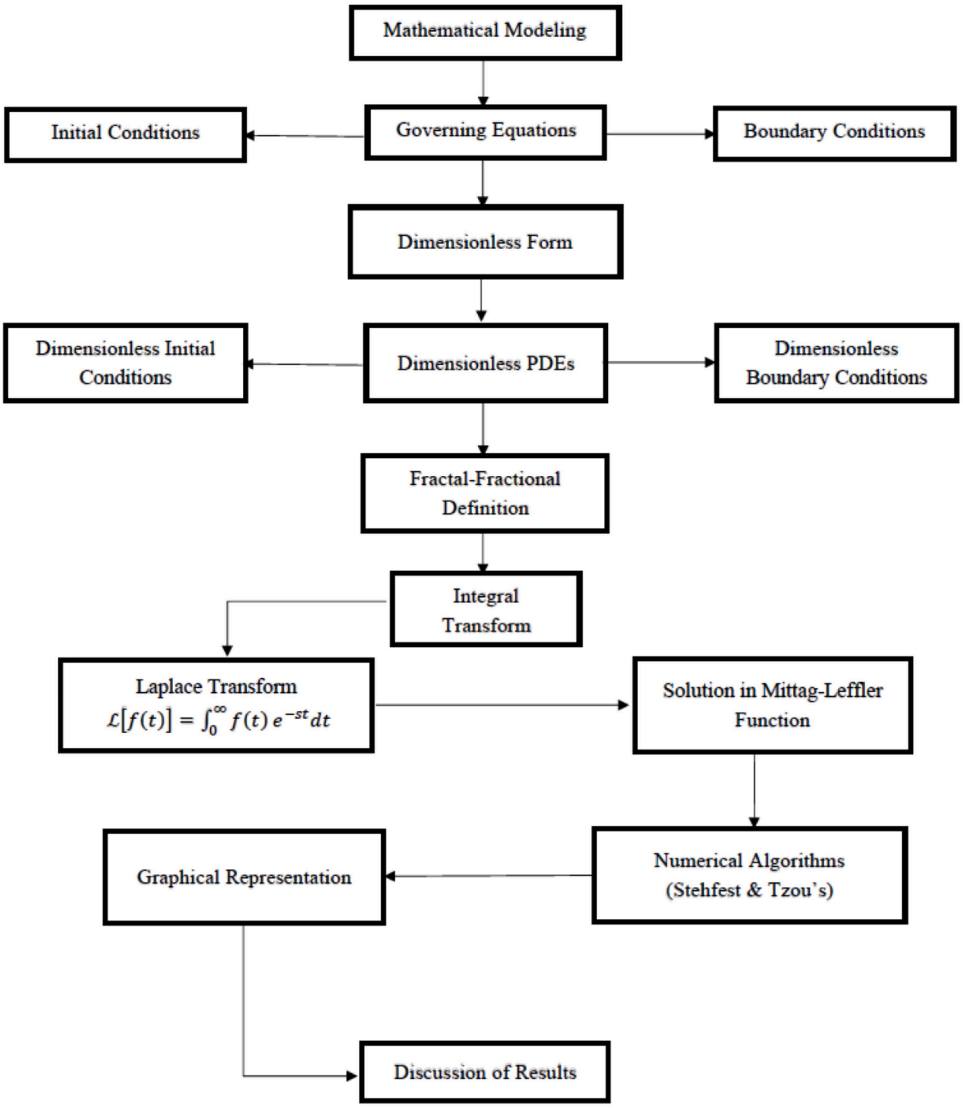

Fig. 2. The model flow chart.

Table 3
Examining the velocity profiles, concentration, and temperature using numerical methods.

y	$\vartheta_1(\xi,t)$ for Stehfest	$\vartheta_1(\xi,t)$ for Tzou's	$\psi_1(\xi,t)$ for Stehfest	$\psi_1(\xi,t)$ for Tzou's	$V_1(\xi,t)$ for Stehfest	$V_1(\xi,t)$ for Tzou's
0.1	0.0763	0.0764	0.0703	0.0716	0.1496	0.1519
0.2	0.1539	0.1542	0.1424	0.1448	0.2891	0.2936
0.3	0.2343	0.2348	0.2177	0.2211	0.4087	0.4149
0.4	0.3185	0.3193	0.2987	0.3024	0.4988	0.5062
0.5	0.4088	0.4095	0.3851	0.3902	0.5508	0.5586
0.6	0.5059	0.5066	0.4814	0.4865	0.5565	0.5643
0.7	0.6118	0.6125	0.5884	0.5933	0.5099	0.5164
0.8	0.7282	0.7287	0.7088	0.7128	0.4043	0.4091
0.9	0.8569	0.8572	0.8450	0.8475	0.2356	0.2381

constraint on the hybrid nanofluid's moving velocity is shown in Fig. 6a. The velocity profile decreases when porosity is increased. Porosity is the volume proportion of empty spaces (pores) in a substance to its overall volume. The variation in velocity is often more consistent throughout the flow field in very porous material. The curve of velocity grows more parabolic as porosity drops, with lower speeds close to the borders and greater velocities in the flow's core. The velocity profile of the Peclet number is shown in Fig. 6b. The velocity profile decreases when the (*Pe*) is increased. A significant (*Pe*) suggests an adjectively dominated distribution, while a small (*Pe*) number shows a diffuse flow. Physically, the (*Pe*) measures the relative significance of the advection of diffusion. The effect of mass and heat Grashof numbers on the velocity profile are shown in Fig. 7a & b. Fig. 7a represents the effect of the heat Grashof number (*Gr*) on fluid flow. As the values of (*Gr*, *Gm*) increase, the velocity increases, as depicted in Fig 7a & b. The concentration gradient rises with increasing (*Gr*, *Gm*) enhancing the buoyant forces. The buoyancy impact brought on by thermal gradients is amplified by the rise in the (*Gr*), which raises fluid velocity close to the heated surface. In

Table 4
Analyzing governed outcomes at various time values.

y	$\vartheta_1(\xi,t)$ at t = 1.0	$\vartheta_1(\xi,t)$ at t = 2.5	$\psi_1(\xi,t)$ at t = 1.0	$\psi_1(\xi,t)$ at t = 2.5	$V_1(\xi,t)$ at t = 1.0	$V_1(\xi,t)$ at t = 2.5
0.1	0.0729	0.0829	0.0658	0.0814	0.0842	0.2392
0.2	0.1474	0.1669	0.1334	0.1640	0.1640	0.4603
0.3	0.2250	0.2528	0.2048	0.2487	0.2351	0.6459
0.4	0.3071	0.3418	0.2820	0.3366	0.2925	0.7803
0.5	0.3956	0.4343	0.3670	0.4289	0.3310	0.8501
0.6	0.4922	0.5329	0.4621	0.5268	0.3447	0.8401
0.7	0.5988	0.6373	0.5700	0.6315	0.3267	0.7583
0.8	0.7174	0.7491	0.6931	0.7443	0.2694	0.5870
0.9	0.8503	0.8696	0.8355	0.8667	0.1639	0.3325

a similar way a greater (Gm) accelerates the fluid flow by amplifying the buoyancy force caused by concentration variations. In situations involving natural convection when buoyancy-driven flow is important, these effects are most noticeable.

Fig. 8a demonstrates the impact of the magnetic field parameter (M) on the velocity profile, showing a reduction in velocity as M increases. This decrease is attributed to the Lorentz force, which resists the fluid flow, leading to lower velocities near the channel walls and significant velocity at the center. Similarly, Fig. 8b highlights the influence of magnetic inclination, where an increase in the inclination angle further diminishes the velocity profile. At a right angle, the magnetic field is strongest, effectively controlling the fluid velocity. Fig. 9a explores the role of nanoparticle volume fraction in hybrid nanofluids, revealing that adding nanoparticles increases the fluid's viscosity and slows the flow. Lastly, Fig. 9b compares the effects of different nanoparticles over time, showcasing their varying influences on the fluid's behavior at different time intervals. Together, these findings underscore the critical roles of magnetic field parameters, inclination angles, and nanoparticle compositions in modulating fluid flow characteristics. It is observed that the fluid velocity of water-base ($CuO + Ag + H_2O$) hybrid nanofluids is more significant as compared to CMC base (CuO + Ag + CMC) hybrid

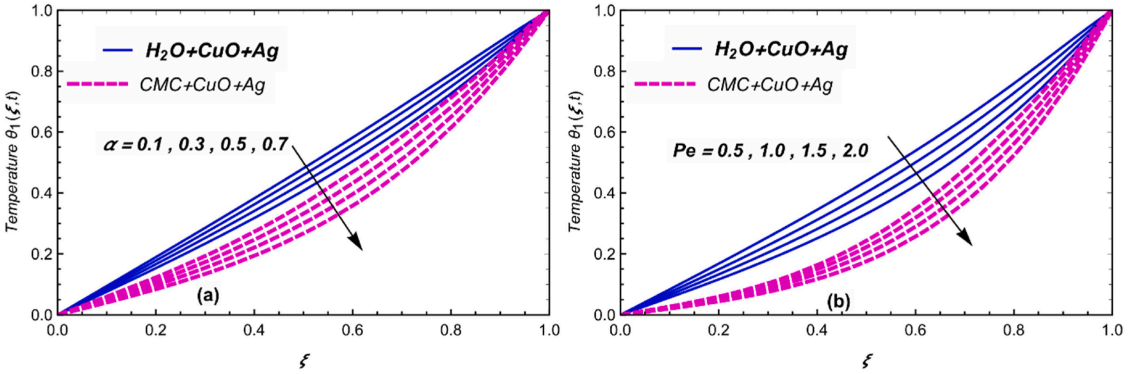

Fig. 3. Effect of a)αand b)*Pe*on momentum profile.

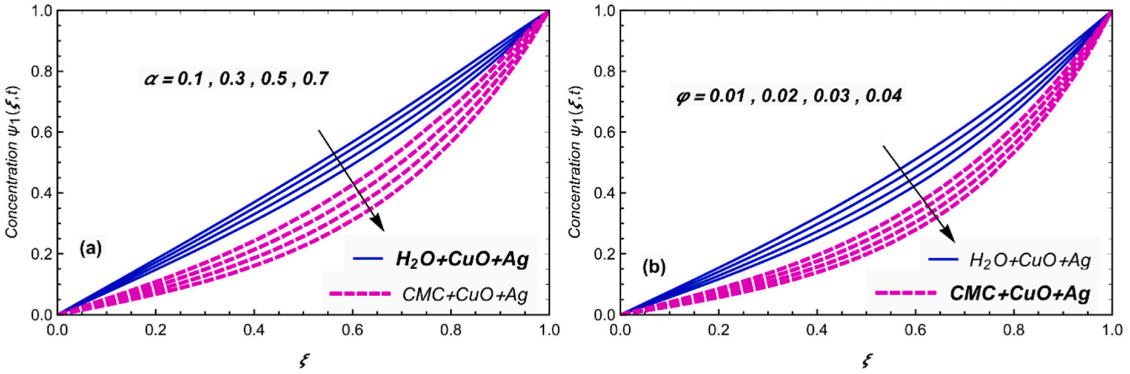

Fig. 4. Effect of a):αand b):φon concentration field.

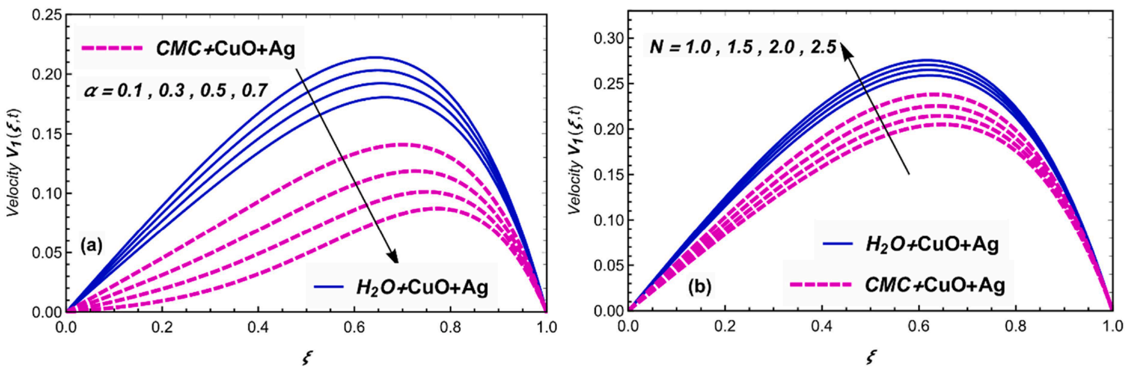

Fig. 5. Effect of a): αand b): *N*on momentum field with $\beta = 0.6,\ Pe = 2.5,\ Gr = 6.5,\ \mathrm{M} = 1.7,\ \theta = \frac{\pi}{6},\ \varphi = 0.03,\ \mathrm{Gm} = 4.6,\ K = 1.5,\ t = 1.0.$

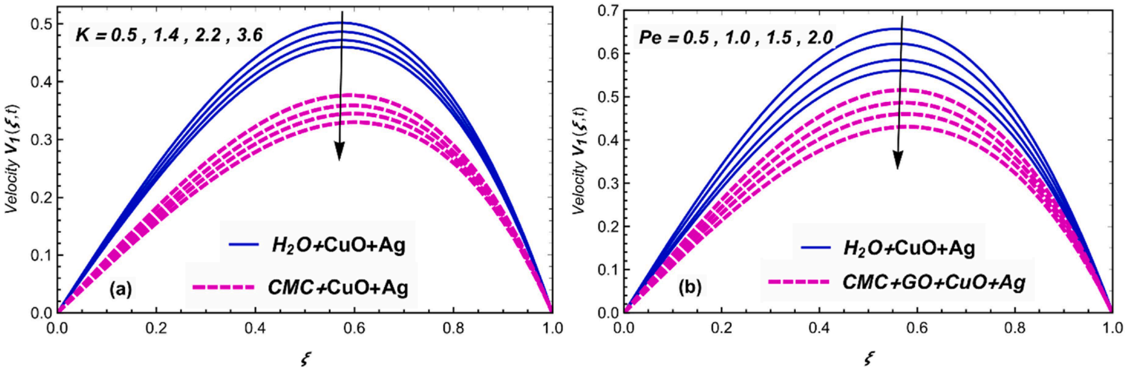

Fig. 6. Effect of a): *K*and b): *Pe*on momentum field with $\alpha,\ \beta = 0.6,\ Gr = 6.5,\ \mathrm{N} = 1.5,\ \mathrm{M} = 1.7,\ \theta = \frac{\pi}{6},\ \varphi = 0.03,\ \mathrm{Gm} = 4.6,\ t = 1.0$.

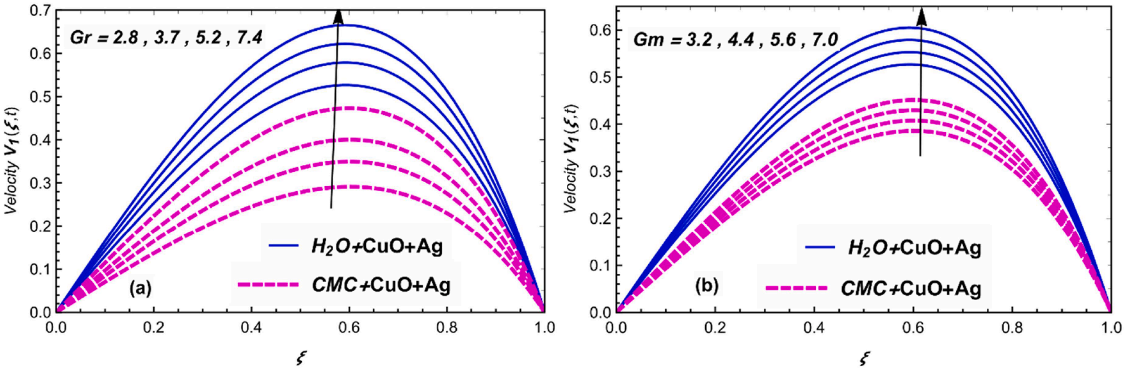

Fig. 7. Effect of a): *Gr*and b): *Gm*on momentum field with $\alpha,\ \beta = 0.6,\ Pe = 2.5,\ \mathrm{N} = 1.5,\ \mathrm{M} = 1.7,\ \theta = \frac{\pi}{6},\ \varphi = 0.03,\ K = 1.5,\ t = 1.0$.

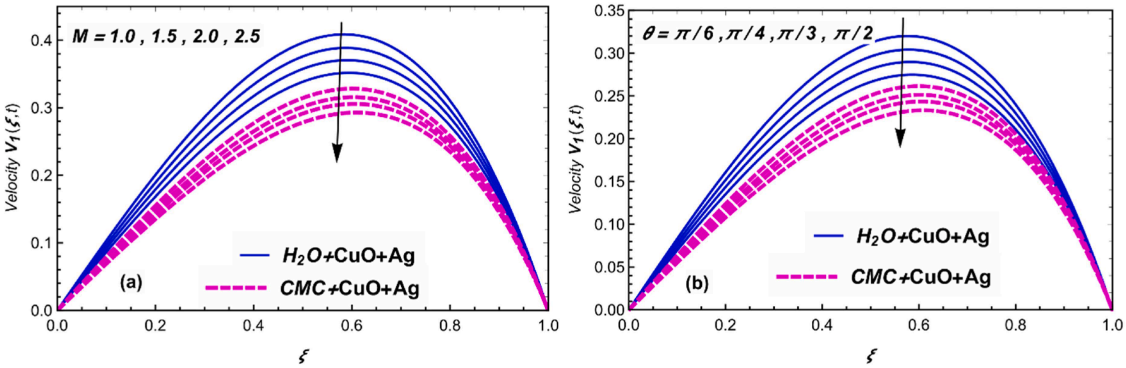

Fig. 8. Effect of a): *M*and b): θon momentum field withα, β = 0.6, *Pe* = 2.5, *Gr* = 6.5, N = 1.5, φ = 0.03, Gm = 4.6, *K* = 1.5, *t* = 1.0.

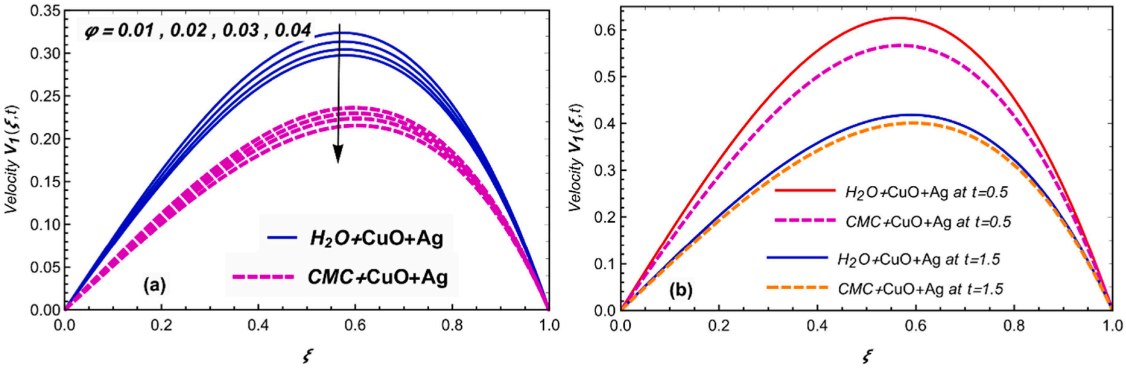

Fig. 9. Effect of a): φand b): comparison of nanofluids on momentum field with $\alpha,\ \beta = 0.6,\ Pe = 2.5,\ Gr = 6.5,\ \mathrm{N} = 1.5,\ \mathrm{M} = 1.7,\ \theta = \frac{\pi}{6},\ \mathrm{Gm} = 4.6,\ K = 1.5,\ t = 1.0$.

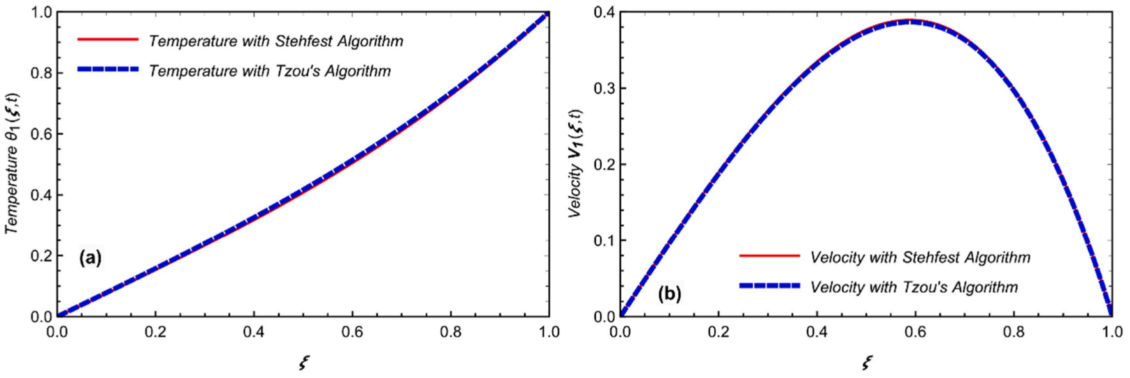

Fig. 10. Graphical comparison of Stehfest and Tzou's numerical algorithms for **a):** temperature field **b):** velocity field.

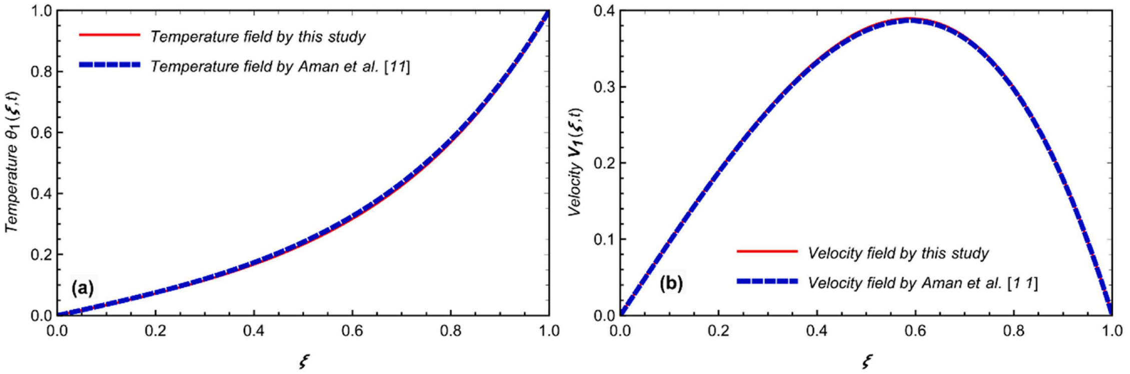

Fig. 11. Comparison of the obtained results with those of Aman et al. [11].

Table 5
Analyzing the Nusselt, skin friction numbers, and Sherwood at various times.

α	*Nu* at t = 1.0	*Nu* at t = 2.5	*Sh* at t = 1.0	*Sh* at t = 2.5	C_f at t = 1.0	C_f at t = 2.5
0.1	0.4908	0.5168	0.4800	0.5049	0.5392	0.6935
0.2	0.4922	0.5397	0.4814	0.5268	0.5689	0.7716
0.3	0.4945	0.5593	0.4837	0.5458	0.6151	0.9208
0.4	0.4973	0.5763	0.4864	0.5619	0.6863	1.2238
0.5	0.5001	0.5901	0.4895	0.5751	0.7875	1.8659
0.6	0.5046	0.6008	0.4936	0.5854	0.9022	3.1317
0.7	0.5106	0.6087	0.4996	0.5929	0.9650	5.0796
0.8	0.5191	0.6137	0.5081	0.5977	0.8451	6.4380
0.9	0.5296	0.6162	0.5188	0.6001	0.3716	2.9231

nanofluids due to the physical characteristics of the considered nanoparticles.

The obtained findings of the directed model are validated and justified by the plotting of Figs. 10(a, b) and 11(a, b). The correctness of our obtained conclusion is demonstrated by the overlap of the two curves in Fig. 10a and b, which compare the numerical methods for momentum and heat fields. Fig. 11a and b compare with Aman et al. [11], and the results are close enough to support our investigation. The numerical analysis of the results at different time values and with different numerical techniques is presented in Tables 3 and 4. Table 3 further supports the validity of this investigation by showing the overlap and proximity of the obtained data. Table 4 shows that as time passes, the momentum profile increases while the temperature and concentration profiles decrease. Furthermore, the numerical comparison of the skin friction, Sherwood number, and Nusselt number for different time values is examined in Table 5, which also demonstrates that all of the major ratios would gradually decrease with time.

6. Conclusions

This study examines the free convective flow of a hybrid nanofluid composed of (CuO) and (Ag) nanoparticles suspended in a mixture of (CMC) and (H_2O) as base fluids. To model the system, the fractal-fractional derivative, a modern and efficient fractional derivative characterization, is employed, and the solution is obtained using the LT technique. Through graphical and numerical analysis, the influence of various parameters on the governing profiles is explored in detail. The results provide insights into the behavior of the hybrid nanofluid under different constraints, highlighting its potential applications and the effectiveness of fractional modeling techniques. Key findings are below summarized to emphasize the study's contributions to hybrid nanofluid dynamics and fractional calculus applications:

- The temperature profile decreases asymptotically over time as the fractal constraints increase, highlighting the impact of fractional parameters on heat dissipation.
- Velocity and concentration profiles similarly decrease with increasing fractional constraint values, demonstrating the influence of fractal characteristics on fluid dynamics.
- Numerical validation is achieved through the alignment of solution curves obtained from two distinct numerical techniques, confirming the accuracy and robustness of the results.
- The buoyancy effects significantly enhance the velocity profile as the (Gr) and the modified (Gr) increase, indicating a direct correlation between buoyancy forces and fluid flow.
- Comparisons between the water (H_2O)-based suspension and the carboxymethyl cellulose (CMC)-based hybrid nanofluids reveal that the former has a stronger influence on the thermal and momentum behavior of the system.

- Validation of the momentum profile is graphically demonstrated by comparing the velocity solutions recorded in this study with those reported by Aman et al. [11], further corroborating the reliability of the findings.
- This study underscores the critical role of fractional parameters, buoyancy effects, and nanoparticle composition in governing the thermal and flow behavior of hybrid nanofluids.
- The dual validation approach reinforces the consistency and applicability of the numerical techniques for analyzing complex systems involving fractal constraints.
- Future work can focus on extending the analysis to different base fluids and exploring more advanced hybrid nanofluid compositions for enhanced thermal performance.

Ethical approval

Not applicable.

Funding

Not applicable.

CRediT authorship contribution statement

Firas Ghanim: Writing – original draft, Investigation, Formal analysis, Conceptualization. **Ali Hasan Ali:** Writing – review & editing, Visualization, Software, Methodology, Formal analysis. **Ghassan Ezzulddin Arif:** Writing – original draft, Resources, Conceptualization. **Ali Raza:** Writing – original draft, Supervision, Methodology, Conceptualization.

Declaration of competing interest

The authors declare that they have no known competing financial interests or personal relationships that could have appeared to influence the work reported in this paper.

Data availability

The datasets used and/or analysed during the current study available from the corresponding author on reasonable request.

References

[1] S.U. Choi, "Nanofluids: from vision to reality through research," 2009.
[2] S.U. Choi, J.A. Eastman, Enhancing Thermal Conductivity of Fluids With Nanoparticles, Argonne National Lab.(ANL), Argonne, ILUnited States, 1995.
[3] R. Ali, M.I. Asjad, A. Akgül, An analysis of a mathematical fractional model of hybrid viscous nanofluids and its application in heat and mass transfer, J. Comput. Appl. Math. 383 (2021) 113096.
[4] M. Ahmad, M.I. Asjad, A. Akgül, and D. Baleanu, "Analytical solutions for free convection flow of casson nanofluid over an infinite vertical plate," 2021.
[5] T. Hayat, S. Asad, A. Alsaedi, Flow of Casson fluid with nanoparticles, Appl. Math. Mech. 37 (2016) 459–470.
[6] M. Sheikholeslami, R. Ellahi, Electrohydrodynamic nanofluid hydrothermal treatment in an enclosure with sinusoidal upper wall, Appl. Sci. 5 (2015) 294–306.
[7] M. Sheikholeslami, Q.Z. Zia, R. Ellahi, Influence of induced magnetic field on free convection of nanofluid considering Koo-Kleinstreuer-Li (KKL) correlation, Appl. Sci. 6 (2016) 324.
[8] C. Milici, G. Drăgănescu, J.T. Machado, Introduction to Fractional Differential Equations, 25, Springer, 2018.
[9] A. Boutiara, M.S. Abdo, M.A. Alqudah, T. Abdeljawad, On a class of Langevin equations in the frame of Caputo function-dependent-kernel fractional derivatives with antiperiodic boundary conditions, AIMS. Math. 6 (2021) 5518–5534.
[10] D. Vieru, C. Fetecau, C. Fetecau, Time-fractional free convection flow near a vertical plate with newtonian heating and mass diffusion, Therm. Sci. 19 (2015) 85–98.
[11] S. Aman, I. Khan, Z. Ismail, M.Z. Salleh, I. Tlili, A new Caputo time fractional model for heat transfer enhancement of water based graphene nanofluid: an application to solar energy, Results. Phys. 9 (2018) 1352–1362.
[12] V.V. Kulish, J.L. Lage, Application of fractional calculus to fluid mechanics, J. Fluids. Eng. 124 (2002) 803–806.
[13] F. Ali, M. Saqib, I. Khan, N.Ahmad Sheikh, Application of Caputo-Fabrizio derivatives to MHD free convection flow of generalized Walters'-B fluid model, Eur. Phys. J. Plus 131 (2016) 377.
[14] W.A. Azhar, D. Vieru, C. Fetecau, Free convection flow of some fractional nanofluids over a moving vertical plate with uniform heat flux and heat source, Phys. Fluids 29 (2017) 082001.
[15] K. Naganthran, M. Mustafa, A. Mushtaq, R. Nazar, Dual solutions for fluid flow over a stretching/shrinking rotating disk subject to variable fluid properties, Physica A: Statist. Mech. Appl. 556 (2020) 124773.
[16] N. Okechi, M. Jalil, S. Asghar, Flow of viscous fluid along an exponentially stretching curved surface, Results. Phys. 7 (2017) 2851–2854.
[17] D. Pal, G. Mandal, Thermal radiation and MHD effects on boundary layer flow of micropolar nanofluid past a stretching sheet with non-uniform heat source/sink, Int. J. Mech. Sci. 126 (2017) 308–318.
[18] M. Ramzan, H. Gul, M. Malik, H.A.S. Ghazwani, Entropy minimization analysis of a partially ionized Casson nanofluid flow over a bidirectional stretching sheet with surface catalyzed reaction, Arab. J. Sci. Eng. (2022) 1–13.
[19] S. Nadeem, R. Mehmood, N.S. Akbar, Oblique stagnation point flow of a Casson-nano fluid towards a stretching surface with heat transfer, J. Comput. Theor. Nanosci. 11 (2014) 1422–1432.
[20] S. Aman, I. Khan, Z. Ismail, M.Z. Salleh, A.S. Alshomrani, M.S. Alghamdi, Magnetic field effect on poiseuille flow and heat transfer of carbon nanotubes along a vertical channel filled with Casson fluid, AIP. Adv. 7 (2017) 015036.
[21] M. Ramzan, H. Gul, S. Kadry, Y.-M. Chu, Role of bioconvection in a three dimensional tangent hyperbolic partially ionized magnetized nanofluid flow with Cattaneo-Christov heat flux and activation energy, Int. Commun. Heat Mass Transf. 120 (2021) 104994.
[22] T. Zubair, S.A. Zanib, M.I. Asjad, A novel definition of the caputo fractional finite difference approach for Maxwell fluid, Comput. Appl. Math. 43 (2024) 238.
[23] Q. Ali, U. Younas, M. Farman, M. Amir, Prabhakar fractional simulation for thermal analysis of magnetohydrodynamics flow of Oldroyd-B fluid using slip and newtonian heating effects, J. Therm. Anal. Calorim. (2024) 1–14.
[24] S. Abbas, Z.U. Nisa, M. Nazar, M. Amjad, H. Ali, A.Z. Jan, Application of heat and mass transfer to convective flow of Casson fluids in a microchannel with Caputo–Fabrizio derivative approach, Arab. J. Sci. Eng. 49 (2024) 1275–1286.
[25] S. Maatoug, K. Al-Khaled, A. Raza, T. Labidi, L. Kolsi, W. Chammam, et al., Fractional computations for free convective flow of Casson-hybrid nanofluid flow with sodium alginate and water as based materials, Int. J. Modern Phys. B 38 (2024) 2450240.
[26] A.M. Abed, H. Shabbir, N. Nigar, A.H. Ali, A. Raza, Inspection of numerical and fractional CMC and water-based hybrid nanofluid with power law and non-singular kernel: a fractal approach, Int. J. Thermofluids 23 (2024) 100772.
[27] A.H. Ali, A. Raza, B. Batiha, A.M. Abed, Z.A. Abduljabbar, Exact and fractional solution of MHD generalized couette hybrid nanofluid flow with Mittag–Leffler and power law kernel, Int. J. Thermofluids 24 (2024) 100837.
[28] P. Mayeli, G.J. Sheard, Buoyancy-driven flows beyond the Boussinesq approximation: a brief review, Int. Commun. Heat Mass Transf. 125 (2021) 105316.
[29] Y.M. Chu, S. Bilal, M.R. Hajizadeh, Hybrid ferrofluid along with MWCNT for augmentation of thermal behavior of fluid during natural convection in a cavity, Math. Methods Appl. Sci. (2020).
[30] B. Fallah, S. Dinarvand, M.Eftekhari Yazdi, M.N. Rostami, I. Pop, MHD flow and heat transfer of SiC-TiO2/DO hybrid nanofluid due to a permeable spinning disk by a novel algorithm, J. Appl. Comput. Mech. 5 (2019) 976–988.
[31] A. Raza, S.U. Khan, M.I. Khan, S. Farid, T. Muhammad, M.I. Khan, et al., Fractional order simulations for the thermal determination of graphene oxide (GO) and molybdenum disulphide (MoS2) nanoparticles with slip effects, Case Stud. Therm. Eng. 28 (2021) 101453.
[32] K. Zheng, A. Raza, A.M. Abed, H. Khursheed, L.F. Seddek, A.H. Ali, et al., New fractional approach for the simulation of (Ag) and (TiO2) mixed hybrid nanofluid flowing through a channel: fractal fractional derivative, Case Stud. Therm. Eng. 45 (2023) 102948.